nature physics

Supplementary information

https://doi.org/10.1038/s41567-024-02716-5

Dynamic forces shape the survival fate of eliminated cells

In the format provided by the authors and unedited

Methods

1 Experimental Methods

1.1 Cell culture and reagents

MDCK WT Type II (ATCC CCL-34) (WT), MDCK LifeAct GFP, MDCK E-cadherin KO (E-cad KO)[1] and MDCK E-cadherin KO LifeAct GFP cells were cultured in DMEM (containing GlutaMAX, high glucose and pyruvate; Life Technologies) supplemented with 10% foetal bovine serum (FBS; Life Technologies) and 1% penicillin-streptomycin (Life Technologies) at 37°C with 5% CO2. MDCK VC3Ai and RC3Ai stable cell lines expressing caspase probe in GFP and RFP respectively was developed using lentiviral transfection[2]. The plasmid was a kind gift from Romain Levayer at Institut Pasteur. Caspase-3 indicator NucView (Abcam) was used for caspase staining (1:100) dilution was used for live imaging and added 30-60mins prior to imaging. Annexin V AF568 (ThermoFisher Scientific) (1:400) was used for staining and added 30-60mins prior to imaging.

1.2 Immunofluorescence staining

Cells were fixed with 4% paraformaldehyde (PFA), permeabilized with 0.5% Triton-X 100 for 5 min, blocked with 1% BSA/PBS for 1 hour, and incubated with primary antibody overnight at 4°C. The samples were then incubated with secondary antibody and Hoescht (1:10,000 and 1:2000 for collagen gels; Thermo Fisher) for 1 hour and mounted on Mowiol 488 (Sigma Aldrich C2081) or Prolong Gold Antifade Mountant (Thermo Fisher) before imaging. The primary antibodies used were directed against activated caspase-3 (1:200; Sigma Aldrich), Myosin IIA (1:100, Abnova), ppMLC (1:100, T18/S19, Cell Signaling, 3674), gp135 (DSHB, 1:20), ZO1 (a gift from Sylvie Robine, 1:50). Anti-mouse, anti-rat and anti-rabbit secondary antibodies conjugated with Alexa (488 or 568; used at 1:200 dilution), Alexa 488 (1:200), Hoescht (1:100) and Alexa 647 (1:50) conjugated phalloidin were purchased from Life Technologies.
Monolayers grown on collagen gels were stained as follows: Cells were fixed with 4% paraformaldehyde (PFA) for 30 min, permeabilized in 0.1% Triton X-100 in PBS for 30 min followed by 3 x 5 min washes. Phalloidin-AF488 (1:200, ThermoFisher) was added over night at 4°C in PBS containing 10% FBS.

1.3 Western blot

Cells are grown in T25 flask until confluency. Thawed Laemmli (Ref: S340-10VL, Sigma Aldrich) and heat it at 98°C for 3min. Rinse the cells on ice with cold PBS twice. Add 500μl of hot laemmli to the cells, scratch the cells and cell lysate (30μg) was loaded onto NuPage 4–12% Bis-Tris gel using a mini gel tank and dry transferred using an iBlot transfer system (Invitrogen).The gels were then blocked using 3% BSA in TBS Tween (0.05%) for 1 hour. The

gels are then left in primary antibody diluted in blocking buffer overnight at 4°Cin a shaker. The gels were then rinsed 3-4 times in TBST for 10 minutes each before incubating them in secondary antibody for 3 hours. The blots were then washed three times with TBST for 10 minutes each. The blots were then revealed using CHEMIDOC MP (BioRad) using Super West Femto (34095 Thermo Scientific).

1.4 Live-cell and fixed-sample imaging

Longterm live imaging was performed using a 10× objective on BioStation IM-Q (Nikon) and a fully automated inverted microscope (Olympus, Japan) at 37°C and 5% CO2. Images are acquired every 10 min or 15 min depending over a period of 24-72 hours. For TFM experiments, phase contrast, fluorescent beads and annexin V (1:400) staining were imaged simultaneously every 5 min. High resolution imaging were performed using Confocal LSM 980 equipped with an Airyscan 2 module and Spinning Disk CSU X1 from Zeiss were used at 40 or 63x oil or water objectives stained with caspase dye (1:100). Images were acquired every 2 min as mentioned in the main text. Extrusion events were considered apoptotic if annexin V or caspase 3 activation occurred within 1 hour of cell extrusion.

1.5 Cytometry analysis of apoptotic and live cell extrusion

In order to characterize the proportion of live and dead cells from a supernatant of extruded cells we used cytometry analysis[3]. Briefly, cells were plated on fibronectin coated 6 well plates and left to spread and grow overnight. Once they reach confluency 24 hours later, the media containing extruded cells were centrifuged at 1,000g for 1 min. The supernatant was removed and replaced with 250μl of dPBS containing 4 μg/ml of Propidium iodide. This mixture was filtered using a 30μm CellTrics strainer to avoid cell clumps, vortexed once and analyzed through the CyAn ADP (Beckman Coulter) analyser system. Cells that die, show membrane rupture allowing the uptake of PI, thereby being PI+ and if the cell membrane is intact then the cells would be PI-. In terms of analysis as shown in Supplementary Fig 1, all the singlets were gated as shown in Supplementary Fig 1a, and fragmented cells were removed using the area as shown in Supplementary Fig 1b. Based on texas red intensity PI+ and PI- cells were identified using the gating strategy employed in Supplementary Fig 1c. The counts were then plotted as shown in Supplementary Fig 1d.

1.6 Growth of 3D cysts

For the growth of cells in 3D cysts, coverslips were coated with a thin layer of 100% matrigel at 4°C and left to polymerize at room temperature. Once matrigel polymerizes, cells were suspended in 100 or 50% matrigel, deposited on the coverslip and left to polymerize in the incubator for 30 min. Once matrigel polymerizes completely, DMEM containing 10% FBS was

added to the cells and left to grow for 10-21 days. Cells were replenished with fresh media every 2 days. Care needs to be taken while changing media to ensure, matrigel does not depolymerize.

1.7 Collagen gel preparation for basal extrusion studies

Type I collagen (Corning), was supplemented with AF647-conjugated type I collagen[4], to make final concentration of 2.1 mg/ml on ice[5]. 150μl of the mix was spread onto a glass bottom dish (FluoroDish, 35 mm, WPI) and let to polymerize at 37°C for 30 min. The gel was equilibrated with 1 ml of culture medium for 4h at 37°C. WT and E-cad KO cells were plated onto the collagen substrates and left to grow for 2 more days to reach confluency and increase density. Media was changed every day to remove cellular debris. They were then live cell imaged by incubating the monolayer with Annexin-V-AF568 (1:400, ThermoFisher) and Hoechst (1:2000, Merck) for 1 hour using scanning scanning confocal microscope equipped with an Airyscan 2 module (LSM 980, Zeiss). Z-stacks were acquired every 15 min for 12 h at 63x magnification.

1.8 Ex-vivo culture of tumour patient derived xenografts and staining

Breast cancer patient derived xenografts were obtained from triple-negative breast tumors (HBCx-60) and generated as previously described[6]. After surgical excision of the tumor xenograft, tumor organoids were isolated[7]. Briefly, tissues were cut into small pieces and digested in RPMI1640 medium supplemented with collagenase 4mg/ml (Sigma-Aldrich) in 10 mM HEPES, 5% FBS, penicillin/streptomycin (1X), Glutamin (1X) for 1 hr at 37°C on a rotating wheel at 150 g. Organoids were pelleted at 400g for 10 min. Then, organoids were incubated for 3-5 min at room temperature (RT) in DMEM/F12 / DNase (2U/μ l). Organoids were pelleted at 400g for 10 min. In order to remove fibroblasts, tumor organoids were washed with DMEM/F12 medium and spinned few times at 400g for 3 seconds at RT until the supernatant is clear. Tumor organoids were resuspended in DMEM with 10 mM HEPES, 5% FBS, 5μg/ml insulin, 10ng/ml Cholera toxin, hydrocortisone 1 mg/ml, penicillin/streptomycin (1X), Glutamin (1X). Around 800 organoids were plated on fluorodish coated with 150µl of Cy5- type I collagen gel for 2-4 days at 37°C. Cells were stained with an anti-Ecadherin ECCD2 (ThermoFisher), phalloidin and Dapi. Metaplastic breast cancer has epithelial (E-cadherin +) and mesenchymal (E-Cadherin -) cancer cells. Only the E-Cadherin negative cellular epitheliums were analyzed.

1.9 Proteomics preparation and mass spectrometry

Cells were grown to 80-90% confluency. Prior to protein extraction, cells were washed twice with PBS and leave them on ice. Cell lysates were extracted using RIPA buffer (50mM Tris-HCl, 150mM NaCl, 2mM EDTA, 10mM $MgCl_2$, 1% NP40, 0.5% Na Deoxycholate, 0.1% SDS, 10% Glycerol) along with protease and phosphatase inhibitor. The lysate is vortexed and left on ice for 20 min. Centrifuge the samples for 1 min at 13,000g at 4°C to remove insoluble debris. Supernatant is collected and protein levels measured using a Pierce BCA Protein Assay

Kit to get about 700-1000μ g/ml of protein per sample. We used 10μg of protein for mass spectometry.

Mass spectometry (MS): MS grade Acetonitrile (ACN), MS grade H_2O and MS grade formic acid (FA) (ThermoFisher Scientific (Waltham, MA, USA)), sequencing grade trypsin (Promega (Madison, WI, USA)), dithiothreitol (DTT) and iodoacetamide (IAA) from Sigma-Aldrich (Saint-Louis, MO, USA) were used during mass spectroscopy. 10 μg of protein sample lysates were mixed with six times volume of cooled acetone (-20°C), vortexed, incubated overnight at -20°C and centrifuged for 10 min at 11,000 g, 4°C the following day. Protein pellets were then dissolved in urea 8M NH_4HCO_3 25mM buffer. Samples were then reduced with DTT 10 mM and alkylated with IAA 20 mM before a 16-fold dilution in 25mM NH_4HCO_3buffer. The pellets were then digestion overnight at 37°C using sequencing grade trypsin (enzyme to sample ratio of 1/20). The digested peptides were loaded and desalted on evotips from Evosep (Odense, Denmark) according to manufacturer's procedure.

LC-MS/MS acquisition: Samples were analyzed on an Orbitrap Fusion mass spectrometer (ThermoFisher Scientific, Waltham, MA, USA) coupled with an Evosep one system (Evosep, Odense, Denmark) operated using the 30SPD method developed by the manufacturer. Briefly, the method includes a 44-min gradient and a total cycle time of 48 min with a C18 analytical column (0.15 x 150 mm, 1.9μm beads, ref EV-1106) which is then equilibrated at room temperature and operated at a flow rate of 500 nl/min. H_2 0.1% FA was used as solvent A and ACN 0.1% FA as solvent B and the mass spectrometer was operated on the data-dependent MS/MS mode. Peptide masses were analyzed on the Orbitrap cell using the full ion scan mode, at a resolution of 120,000, with a mass range of m/z 350-1550 and an AGC target of $4x10^5$. MS/MS was then performed at the top speed 3s mode. Fragmented peptides were selected for fragmentation by Higher-energy C-trap Dissociation (HCD) with a Normalized Collisional Energy of 27% and dynamic exclusion for 60 seconds. Mass fragmentation was measured in an Ion trap in the rapid mode, with an AGC target of $1x10^4$. Monocharged peptides and unassigned charge states were excluded from the MS/MS acquisition. The maximum ion accumulation time was set to 100 ms for MS and 35 ms for MS/MS acquisitions respectively.

Data analysis: Label Free quantitation was performed using Progenesis QI for proteomics software (version 4.2) (Waters, Milford, MA, USA). The software was used to automatically align data to a known reference chromatogram to minimize missing data points. The default settings were used to identify peaks and hence detect features in the raw MS files. The most suitable reference was chosen by the software to normalize the data. The experiment was designed to choose four biological replicates. MS/MS spectra were exported and proteins were identified using PEAKS STUDIO Xpro software (Bioinformatics Solutions Inc., Waterloo, ON, Canada). De Novo was run using the following parameters: trypsin as enzyme (specific), carbamidomethylation (C) as fixed and deamidation (NQ)/oxidation (M) as variable modifications. Precursor and fragment mass tolerances were set as 15 ppm and 0.5 Da respectively. Proteins were matched against the Uniprot Canis Lupus reference proteome FASTA file (release 2021_03, 45351 entries) with a maximum of 2 missed cleavage. The maximum of variable PTM per peptide was set to 4. The spectra data was filtered using a 1% FDR. The identified

results were converted from peptide-based data to protein expression data using the Hi-3 based protein quantification method in Progenesis. Multivariate statistics on protein measurements were performed using Qlucore Omics Explorer 3.7 (Qlucore AB, Lund, SWEDEN). A positive threshold value of 1 was specified to enable a log2 transformation of abundance data prior to normalization i.e. all abundance data values below the threshold was replaced by 1 before transformation. Statistical analysis was performed on the transformed data (i.e. evaluation of differentially present proteins between two groups) using a Student's bilateral t-test and we assume equal variance between groups. A p-value better than 0.01 was used to filter differential candidates.

1.10 RNA sequencing preparation and analysis

RNA was extracted using RNeasy kit (Qiagen, Cat.No./ID:74104) using the manufacturer's protocol. Briefly, cells were harvested and mixed with RLT buffer, disrupted and homogenized using QIAShredder to obtain 2.698 μg/μl (WT) and 0.705 μg/μl of RNA. RNA concentrations were measured using nanodrop or a fluorometric Qubit RNA assay (Life Technologies, Grand Island, New York, USA). The quality of RNA (RNA integrity number) was measured using Agilent 2100 Bioanalyzer (Agilent Technologies, Palo Alto, CA, USA) as per the manufacturer's instructions. To construct the sequencing library, 250 ng of high quality of the total RNA of each sample ($RIN > 8$) was processed using Stranded mRNA Prep kit (Illumina) according to manufacturer instructions. Briefly, after purification of poly-A containing mRNA molecules, mRNA molecules are fragmented and reverse- transcribed using random primers. Replacement of dTTP by dUTP during the second strand synthesis will permit to achieve the strand specificity. Addition of a single A base to the cDNA is followed by ligation of Illumina adapters. Libraries were quantified by Q bit and profiles were assessed using the DNA High Sensitivity LabChip kit on an Agilent Bioanalyzer. Libraries were sequenced on an Illumina Nextseq 500 instrument using 75 base-lengths read V2 chemistry in a paired-end mode. After sequencing, a primary analysis based on AOZAN software (ENS, Paris) was applied to demultiplex and control the quality of the raw data (based of FastQC modules / version 0.11.5). Obtained fastq files were then aligned using STAR algorithm (version 2.5.2b) and quality control of the alignment obtained with Picard tools (version 2.8.1). Reads were then counted using Featurecount (version Rsubread 1.24.1) and the statistical analyses on the read counts were performed with the DESeq2 package version 1.14.1 to determine the proportion of differentially expressed genes between the two conditions. From the initial DESeq2 file containing 11191 genes without duplicates, we then performed the Gene Set Enrichment Analysis with the ClusterProfiler package on R[8]. We used the canis familiaris (Cf) annotation and performed the GSEA from ENSEMBL to SYMBOL annotations without permutation and with p-value and p-value adjusted cutoffs set at 0.05. With this method we identified 225 different GO terms corresponding to 53 upregulated and 152 downregulated genes in the E-cadherin KO compared to the WT condition. We then looked at the Molecular Signatures Database (MSigDB) to find if these up or downregulated genes were present in the gene sets related to specific cellular processes as cell-cell adhesion or

cell death, apoptosis and oxidative stress or cell substrate adhesion regulation[9,10].

1.11 TEER measurements

Cells were grown to confluency on permeable Transwell polyester filters (Costar, Corning incorporated Ref. 3470), and transepithelial electrical resistance (TEER) was measured by EVOM3 Volt/Ohm meter (WPI, USA). Background resistance was measured using cell-free filters which was subtracted by the software. An insert of 6.5mm diameter and 0.4μm pore size was used to grow these cells. Resistance obtained is then calculated for the total area as Ohm. cm^2. Measurements were taken at 24 and 48 hour period for the same sample after media change.

1.12 Preparation of PDMS based traction force microscopy (TFM) substrates

In order to measure traction forces exerted on the substrate, we used soft silicone substrates embedded with beads. First, the substrates are prepared by mixing CyA and CyB components of PDMS (Dow Corning) at 1:1 ratio and spin coated onto plastic dishes to ensure we obtain a flat surface roughly of height 100μm and stiffness 15kPa. We need to maintain this range of substrate thickness as the algorithm used for TFM computation from the displacement of beads assumes the gel to be an infinite half plane surface[11]. We used this PDMS instead of Sylgard for traction force measurements since they are found to behave as an elastic material in this stiffness range. In addition, we are able to control their rigidity thereby enabling us to visualize bead displacement. The substrates are then cured at 80°C for 2 hours. Once cured, the substrates can be stored in dark for a few weeks prior to bead coating. Next, the substrates are silanized with 10% (3-Aminopropyl)triethoxysilane in ethanol for 10 min. The surface is then functionalized with 200nm carboxylated fluorescent beads in the dilution 1:500 in DI water. The substrates are then coated with 50μ/ml of fibronectin for 1 hour prior to cell seeding. Between each step the substrate is washed with PBS or DI water 2-3 times and dried. Once the substrate has been coated with fibronectin the sample should never be left dry and cells need to be seeded immediately. Once the cells are seeded they are left to attach for 1-2 hours and washed with fresh media to remove unattached cells. The cells are left overnight to spread and imaged next day. At the end of the experiment, cells are treated with 10% SDS to detach cells and obtain the relaxed position of beads.

1.13 Atomic force microscopy (AFM) measurement

Local cell stiffness across the apical cell surface and cell-cell junctions of confluent MDCK WT and Ecad KO monolayers were obtained through AFM. For this, the monolayers were subject to AFM indentation using the fast scan mode. The PeakForce QNM-Live Cell (catalog number RP3674160) probe with a probe tip size of 70nm and stiffness (k=0.099 N/m, obtained from manufacturer). Indentations were done with a maximum depth of 600 nm and an approach

speed of 100 μm/s. The local cell stiffness was analyzed using a custom-made MATLAB code available on github (https://github.com/bryantdoss/matlab-afm-indentation).

1.14 Image Analysis

1.14.1 Classification of live or dead extrusions from live imaging

An extrusion event is defined as a cell that is expelled from a monolayer and seems to be detached from the monolayer for a couple of frames. Cells are removed from the monolayer even during cell division, however they re-enter the monolayer in 1-2 frames. However, during an extrusion event, cells are expelled out of the monolayer and very rarely re-insert into the monolayer. These events are marked using a point tool on ImageJ and stored as ROI's for future reference. The area, of these extruded cells, and surrounding neighbours are then calculated through manual segmentation. The change in area of these cells are often plotted as a function of time before the extrusion event. Long term imaging and live vs apoptotic cell extrusion were quantified as follows. Brightfield images of cell monolayers as well as fluorescent images of the annexin-V-AF647 and the Hoechst signal were acquired every 15 min for 48 h. A random forest classifier was trained using the pixel classification workflow in ilastik[12] to automatically segment extrusion events in brightfield timelapse movies. Using ilastik, another classifier was trained to automatically segment annexin-positive extrusions based on Annexin V Alexa Fluor 647 (Thermo Fisher) signal. The outputs were smoothed with a 2x2 median filter, processed using the watershed algorithm and merged. A third classifier was trained to classify live (= annexin negative) and dead (= annexin positive) extrusions based on the merged pre-processed images, resulting in a three-intensity image. Thus, a change of cell fate of an extruded cell from live to dead was reflected in an intensity change. In ImageJ, TrackMate[13] was used to detect and track extrusions in the three-intensity image using the label detector. The extrusion positions were determined, and the fate of the extruded cell was followed in time and space. Extrusion events which stayed annexin-negative for 30 min were classified as live extrusions. Extrusions were counted and the ratios between live and dead cells were calculated.

1.14.2 Velocity and strain rate measurements

Velocities of single cells have been manually tracked using ImageJ. However, within a monolayer, manual tracking of individual cells from phase contrast imaging can be time consuming and prone to errors. Thus in this work we employ a technique called Particle Image Velocimetry (PIV) extensively used in fluid dynamics to track the displacement of cells within a monolayer. There are two main tools used in biological studies namely, matPIV and PIVlab. In this work, PIVlab[14] was used due to the availability of extensive online tutorials and the presence of a GUI making it more user friendly. In PIV, a given image is divided into windows of a specified size with a specified overlap. In a given window, the peak in intensity is identified and using a Fast Fourier Transform (FFT) based cross-correlation function between subsequent frames, the most probable displacement of particles within this window is obtained. This method estimates

the average deformation field within a given interrogation window and gives a pretty decent estimate of the velocity of cells within the monolayer and has been widely used in various collective migration studies. Velocity measurements were obtained mainly from phase contrast images since you can observe changes in intensity within the cell. In this work a window size of 64x64 and 32x32 pixels with an overlap of 50% was used to obtain cellular velocity at 10x magnification. This was scaled accordingly for high magnifications. From the displacement fields obtained, we can then calculate the strain rate as $\dot{\varepsilon} = \nabla \mathbf{v}$.

1.14.3 Force and stress measurements

In order to measure the forces exerted by cells on the substrate, the deformation field of beads are first obtained using a PIV window size of 32 x 32 (20μm) pixels and a 50% overlap at 10x or 20x magnification. The displacement fields are then transformed into traction forces using Fourier Transform traction cytometry (FTTC)[15] by inputting the stiffness of the substrate used and poisson's ratio of 0.5 for viscoelastic substrates. The regularization parameter is a term used to minimize noise and this is set to 9e-9 in this work based on[15]. Due to force balance, forces estimated at the boundary can give rise to erroneous values and the traction forces in a width of about 10-15 μm in the image boundary were discarded. The stress field within the epithelial monolayer was estimated by inverting the force balance equation irrespective of epithelial rheology using Bayesian Inference Stress Microscopy (BISM)[16]. A positive value of isotropic stress (negative pressure) indicates tension while a negative stress (positive pressure) indicates compression.

1.14.4 Collagen gel z-projection

Within the ZEN software, an automated deconvolution was performed. 3D projections were generated using ImageJ.

2 Computational model

2.1 3D computational model of the cell monolayer

We use a recently developed three-dimensional (3D) phase-field model for active cell layers[17]. Within this framework cells are represented as 3D deformable particles, which dynamically adapt their shape in response to active stresses, and interaction forces with other cells and the underlying substrate. In this vein, we consider a cellular monolayer consisting of N cells on a rigid substrate with its surface normal $\vec{e}_n\,(=\vec{e}_z) = \vec{e}_x \times \vec{e}_y$ and periodic boundaries in both $\vec{e}_x$ and $\vec{e}_y$, where $(\vec{e}_x, \vec{e}_y, \vec{e}_z)$ constitute the global orthonormal basis. Each cell i is represented by a three-dimensional (3D) phase-field, $\phi_i = \phi_i\,(\vec{x}, t)$ and initialized with radius R_0. The dynamics associated with relaxation of cell interface follows a time-dependent Ginzburg-Landau model,

categorized as *model* A in the theory of dynamics critical phenomena[18], with an extra advective term:

$$\partial_t \phi_i + \vec{v}_i \cdot \vec{\nabla}\phi_i = -\Gamma \frac{\delta \mathcal{F}}{\delta \phi_i}, \qquad i = 1, ..., N \tag{1}$$

Based on the definition for free energy functional $\mathcal{F}$ (see Eq. 2), ϕ_i continuously varies between $\phi = 1$ and $\phi = 0$ through a diffusive interface of length λ. Γ is the mobility coefficient, affecting the relaxation time scale (see section 2.3 in *Methods*). Furthermore, the advective term $\vec{v}_i \cdot \vec{\nabla}\phi_i$ updates the location of $\phi_i\left(\vec{x}, t\right)$ for each time step and each cell i with velocity $\vec{v}_i$.

The free energy functional reads[17]:

$$\begin{aligned}
\mathcal{F} &= \sum_i^N \frac{\gamma^i}{\lambda} \int d\vec{x} \{ 4\phi_i^2 \left(1-\phi_i\right)^2 + \lambda^2 \left(\vec{\nabla}\phi_i\right)^2 \} \\
&+ \sum_i^N \mu \left(1 - \frac{1}{V_0} \int d\vec{x} \phi_i^2\right)^2 + \sum_i^N \sum_{j \neq i} \frac{\kappa_{\text{cc}}}{\lambda^2} \int d\vec{x} \phi_i^2 \phi_j^2 \\
&+ \sum_i^N \sum_{j \neq i} \omega_{\text{cc}}^i \int d\vec{x} \vec{\nabla}\phi_i \cdot \vec{\nabla}\phi_j + \sum_i^N \frac{\kappa_{\text{cs}}}{\lambda^2} \int d\vec{x} \phi_i^2 \phi_w^2 \\
&+ \sum_i^N \omega_{\text{cs}}^i \int d\vec{x} \vec{\nabla}\phi_i \cdot \vec{\nabla}\phi_w .
\end{aligned} \tag{2}$$

As such the free energy stabilizes cell interface and includes mechanical properties of the cells such as cell cortex tension (γ^i), as well as gradient contributions ($\vec{\nabla}\phi$) that account for, and distinguish between, cell-cell (ω_{cc}^i) and cell-substrate (ω_{cs}^i) adhesions. In addition to the cortex tension and adhesion terms, compressibility (μ), puts a soft constraint on the cell volume[19–22] around $V_0 = (4/3)\pi R_0^3$ and κ captures repulsion between cell-cell (subscript cc) and cell-substrate (subscript cs) and ϕ_w denotes a static phase-field representing the substrate. Based on this free energy functional, the interior and exterior of cell i corresponds to $\phi_i = 1$ and $\phi_i = 0$, respectively, connected by a diffuse interface parameterized by a length λ. Thus, the contribution due to adhesive cell-cell interactions are captured as follows:

$$\mathcal{F}_{\substack{\text{adhesion} \\ \text{cell-cell (cc)}}} = \sum_i^N \sum_{i \neq j} \omega_{\text{cc}}^i \int d\vec{x} \vec{\nabla}\phi_i \cdot \vec{\nabla}\phi_j \tag{3}$$

This expression only contributes by decreasing the energy when the gradients of phase-fields i and j spatially and temporally overlap. For each phase-field, the gradient is only non-zero at the interface. This is different than the repulsive interactions with a quadratic form and based on the overlap of phase-fields and not their gradients. In a similar form, we also define a cell-substrate adhesion where the substrate is represented by a static phase-field ϕ_w:

$$\mathcal{F}_{\substack{\text{adhesion} \\ \text{cell-substrate (cs)}}} = \sum_i^N \omega_{\text{cs}}^i \int d\vec{x} \vec{\nabla}\phi_i \cdot \vec{\nabla}\phi_w \tag{4}$$

To resolve the forces generated at the cellular interfaces, we utilize an overdamped dynamics:

$$\vec{t}_i = \xi \vec{v}_i - \vec{F}_i^{\text{sp}} = -\int d\vec{x} \left(\mathbf{\Pi}^{\text{int}} \cdot \vec{\nabla} \phi_i \right) \tag{5}$$

where $\mathbf{\Pi}^{\text{int}} = \left(\sum_i -(\delta \mathcal{F}/\delta \phi_i)\right) \mathbf{1} + \left(\sum_i -(\zeta^i \phi_i \boldsymbol{Q}_i)\right)$, in which the active stress is defined according to the previously published comparison of WT and E-cad KO cells[1] and ζ^i sets the strength of active nematics stresses, with negative sign indicating contractile stresses[23].

Furthermore, the the polarization dynamics is introduced based on contact inhibition of locomotion (CIL)[24,25] by aligning the polarity of the cell to the direction of the total interaction force acting on the cell[26,27]. As such, the polarization dynamics is given by:

$$\partial_t \theta_i = -\frac{1}{\tau_{\text{pol}}} \Delta\Theta_i + D_r \eta(t), \tag{6}$$

where $\theta_i \in [-\pi, \pi]$ is the angle associated with polarity vector, $\vec{p}_i = (\cos\theta_i, \sin\theta_i, 0)$ and $\eta(t)$ is a standard Gaussian white noise with zero mean, unit variance, D_r is rotational diffusivity, $\Delta\Theta_i$ is the angle between $\vec{p}_i$ and $\vec{t}_i$, and positive constant τ_{pol} sets the alignment time scale. This model of alignment has the advantage that (a) it contains an explicit timescale and (b) does not require that a cell 'knows' about the position of its neighbours. In addition, this model of alignment has the advantage that it has been parameterized by quantitative comparison to experiments on epithelial cells[27], where it was shown that the contribution from rotational noise is negligible compared to the alignment contribution. As such, in this paper we set $D_r = 10^{-4}$ to a small value. Implicit in our formulation is the assumption of time-scale separability between the dynamics captured by Eq. 5 and Eq. 1. This is justified given the experimental relaxation time scale on the order of seconds (see section 2.3 in *Methods*) and the translational time scale on the order of minutes (see section 2.2 in *Methods*).

Finally, we compute a coarse-grained stress field[28,29] $\boldsymbol{\sigma} = \boldsymbol{\sigma}(\vec{x}, t)$ that encodes both active and passive contributions on a discretized domain, for node i:

$$\boldsymbol{\sigma}^i = \frac{1}{V_{\text{cg}}} \sum_{j \in \Omega_{\text{cg}}} \vec{r}^{ij} \otimes \vec{t}^j \tag{7}$$

where $V_{\text{cg}} = \ell_{\text{cg}}^3$ is the volume corresponding to the coarse-grained length ℓ_{cg} and discretized domain Ω_{cg}, where $(i, j) \in \Omega_{\text{cg}}$, and $\vec{r}^{ij} = (\vec{x}^i - \vec{x}^j)$. Given the definition of active traction for cell i, $\vec{t}_i$, the coarse grained stress field contains contributions from both active and passive forces. Herein, the stress fields are computed using $\ell_{\text{stress}} = a_0$, where grid size $a_0 = 1$.

2.2 Model parameters

2.2.1 Dimensionless groups and sensitivity analyses

In order to facilitate a more effective comparison between models and experiments, the model parameters have been transformed into dimensionless groups (Table I). To do this, we leverage

Dimensionless parameter	Physical interpretation	Sensitivity analyses
λ/R_0	diffuse interface width compared to cell radius	not-sensitive: the width of the diffuse interface is set smaller than the cell radius ($\lambda/R_0 \ll 1$)
$\kappa R_0^2/\mu$	cell-cell overlap to compressibility ratio	not-sensitive: only needed for keeping cell integrity and avoiding overlaps between phase fields
κ_{cc}/κ_{cs}	cell-cell to cell-substrate repulsion energy ratio	not-sensitive: only needed to avoid overlap between phase fields representing cells and substrate
ω_{cc}/ω_{cs}	cell-cell to cell-substrate adhesion energy ratio	one of the main control parameters
$\zeta R_0/\gamma$	contractility to stiffness ratio	one of the main control parameters
$\alpha\tau_{\text{pol.}}/(\xi R_0)$	ratio of realignment to directed motion time	not-sensitive: drives flocking behavior

Table 1: Dimensionless model parameters and their physical interpretation.

the well-established Buckingham-Pi theorem[39,40] that allows reducing the complex physical problems to their simplest possible form by reducing the number of relevant parameters to the independent dimensionless groups. We then vary these dimensionless parameters to conduct a sensitivity analyses which determines the most relevant controlling parameters. The results of the sensitivity analyses are presented in Extended Fig. 7 and are summarized in Table S1. Specifically, we performed a sensitivity analysis to establish the influence of various modeling parameters on the statistics of the isotropic stress field, specifically its mean and susceptibility. The results are shown in Extended Fig. 7a for adhesion ratio ω_{cc}/ω_{cs}, Extended Fig. 7b for activity to elasticity ratio $\zeta R_0/\gamma$ and Extended Fig. 7c for dimensionless compressibility $\kappa R_0/\mu$. For each case, we vary the target parameter while isolating the other parameters. Both the mean and susceptibility have been normalized by the bench case, i.e. the value corresponding to the lowest in the set of values for each parametric study. As expected, the model is not sensitive to compressibility parameter (consistent with previous independent studies of 3D phase field models[41]), slightly sensitive to cell-cell and cell-substrate parameters and most sensitive to the elasticity parameter as manifested in ~ 8 fold increase in the value of the mean field relative to the bench case.

The results of these sensitivity analyses are consistent with previous sensitivity analyses in 2D[1,22,27], which showed that the ratio of active to elastic forces, $(\zeta R_0)/\gamma$, is the predominant factor in governing cell deformation. In the 3D formulation, the ratio of the cell-cell to cell-substrate adhesion, ω_{cc}/ω_{cs}, is an additional significant parameter that affects collective cell motion in monolayers. We further emphasize that the other dimensionless parameter in Table. II, which characterizes the ratio of realignment time to directed motion time sets transition to a flocking state. Since no flocking is observed in these experiments we have chosen this parameter such that flocking is avoided in the simulations.

Simulation parameter	Physical meaning	Numerical value	Mapping to physical units	Measured physical value
R_0	initial cell radius	8	$15\mu m$	$10-20\mu m$ [this study]
γ	cortex tension	$0.008-0.016$	$800-1600pN/\mu m$	$1000-2000pN/\mu m$[30,31]
ξ	friction coefficient	1	$600nN.s/\mu m$	$O(10^2)nN.s/\mu m$[32,33]
ω_{cc}	cell-cell adhesion force	$0.006-0.012$	$12-24nN$	$O(10^1-10^2)nN$[34]
ω_{cs}	cell-substrate adhesion force	$0.001-0.002$	$2-4nN$	$O(10^1-10^2)nN$[35,36]
ζ	active stress	$0.00001-0.001$	$0.5-50Pa$	$O(10^0-10^1)Pa$ [this study]
$\tau_{pol.}$	cell polarity alignment time	200	$20min$	$O(10^1 min)$[37]
α	single cell traction magnitude	0.05	$10nN$	$1-30nN$[38]
κ_{cc}	cell-cell repulsion force	0.5	$--$	$--$
κ_{cs}	cell-substrate repulsion force	0.15	$--$	$--$
μ	stiffness of volume constraint	45	$--$	$--$
λ	width of diffuse interface	1.5	$--$	$--$

Table 2: Mapping of model parameters to physical units. '$--$' indicates that mapping to physical units is non-applicable, since the parameter is model specific, and no experimental measurement is available. Note that in[32,33] the friction coefficient is mapped by using Pa units for force, giving friction dimensions of $nN.s/\mu m^3$, and is here converted to $nN.s/\mu m$ using the cell size as the relevant length scale. The connection between simulation parameters and physical units for active stress depends on the strength of active stress and not whether it is contractile ($0<$) or extensile ($0>$).

2.2.2 Simulation parameters and mapping to physical units

The precise matching of physical model parameters to biological systems is an outstanding challenge. Yet, in our earlier studies using the phase field model, we have successfully applied the cell-based model to reproduce flow fields and mechanical stresses around topological defects[1]. In addition, our comparison with experiments on confined epithelial layers shows that this method can quantitatively capture the amplitude and period of collective oscillations[27]. As such, we have chosen parameters of the models in the range that have proven successful in capturing relevant time, length scales as well as the physical forces in our experiments on epithelial cells. Furthermore, using the cell length, cell velocity, and force units from experiments the simulation length, time, and force units can be mapped into the physical units of $\delta L \sim 2\mu m$, $\delta t \sim 0.1min$, and $\delta F \sim 200nN$, respectively. Using these length, time, and force scales, we have now provided a direct mapping of model parameters to physically relevant units, summarized in the Table II.

2.2.3 Simulation Setup: live vs. apoptotic extrusion

We consider a cellular monolayer consisting of $N = 64$ cells on a substrate with its surface normal $\vec{e}_n\,(=\vec{e}_z) = \vec{e}_x \times \vec{e}_y$ and periodic boundaries in both $\vec{e}_x$ and $\vec{e}_y$, where $(\vec{e}_x, \vec{e}_y, \vec{e}_z)$ constitute the global orthonormal basis. Cells are initiated on a two-dimensional simple cubic lattice and inside a cuboid of size $L_x = L_y = 128$, $L_z = 64$. To capture the natural variations in the physical properties of cells and their environment, we consider cell stiffness, γ^i, cell-cell adhesion, ω^i_{cc}, cell-substrate adhesion, ω^i_{cs}, strength of intercellular active stresses, ζ^i_S and

strength of cell-substrate active stress, ζ_Q^i as random variables that follow a Gaussian distribution, i.e. $x \sim \mathcal{N}(\tilde{\mu}, \tilde{\sigma}^2)$. In particular, we impose the mean value, $\tilde{\mu}$, and the coefficient of variation, $\tilde{\mu}/\tilde{\sigma} = 0.3$, where $\tilde{\sigma}$ is the standard deviation. For the mWT cells, the mean values are: $\zeta_S = +2\text{E} - 5$, $\gamma = 0.008$, $\omega_{\text{cs}} = 0.001$ and $\omega_{\text{cc}} = 0.012$. For the mE-cad KO cells, the mean values are: $\zeta_Q = -0.0006$, $\gamma = 0.016$, $\omega_{\text{cs}} = 0.002$ and $\omega_{\text{cc}} = 0.006$.

2.2.4 Simulation Setup: apical vs. basal extrusion

We consider $N = 25$ cells centered on the substrate with a square whole at the center of size $0.625R_0$ with homogeneous properties, including $\alpha = 0$, $\gamma = 0.008$, $\omega_{\text{cs}} = 0.002$, $\mu = 45$, $\zeta_S = 0$, $\kappa_{\text{cc}} = 0.5$ and $\kappa_{\text{cs}} = 0.15$. This setup, with the hole, is to reproduce the experimental condition with porous, collagen gels. We vary the strength of the normalized strength of active cell-substrate interaction $\tilde{\zeta}_Q = \zeta_Q \times (R_0/(\gamma))$ and the normalized cell-cell adhesion $\omega_{\text{cc}}/\omega_{\text{cs}}$.

2.3 Elastic relaxation time

We studied shape relaxation times, experimentally as well as theoretically. These measurements were performed on cell monolayers grown to confluency on a petridish, using a nanoindenter (Chiaro, Optics 11) mounted on an optical inverted microscope. Cells were indented 1 µm at a rate of 1 m/s using a cantilever with a stiffness $k = 0.022$ N/m and a tip radius of 23.5 m and the data were used to compute the Young's modulus. The constant indentation control was guaranteed using the system's built-in dynamic mode, allowing for a precise positioning while cells were left to relax during 20 seconds. The measured load vs. time was then analyzed and fitted to a General Maxwell Model with 3 elements to compute the relaxation times, using a homemade Python code[42]. The experimental relaxation times are consistent with our theoretical prediction, i.e. higher for WT cells, in the range of 2-20 seconds.
We also compare the experimentally measured relaxation times to our predictions, based on our theoretical analysis and computational model. In the main text we only mentioned the proportionality, without discussing the exact form. Indeed, the elastic shape relaxation time of a cell can be estimated via a linear stability analysis. Specifically, we study the stability due to a small perturbation, $\delta\phi_i$:

$$\delta\phi_i = \epsilon \exp\left(-t/t_{\text{shape}} + iqx\right) \tag{8}$$

where ϵ is the perturbation amplitude, q, is the associated wavenumber and t_{shape} represents the relaxation time. By substituting the above equation into the first part of the free energy functional, i.e. Eq. 2, and applying that to the dynamics described by Eq. 1, we readily find after linearizing the results:

$$t_{\text{shape}} = \left(\frac{\gamma\Gamma\epsilon}{\lambda}\right)^{-1}\left(\frac{1}{8 + 2q^2\lambda^2}\right). \tag{9}$$

This is the basis for $t_{\text{shape}} \propto \gamma^{-1}$. Using the above equation for t_{shape}, and the mapping from the simulation parameters to physical units described in Section 2.2.2, the relaxation time of the

computational model is in the order of $O(10^1 - 10^2)s$, in the same range as in the experiments. Furthermore, to falsify our hypothesis that long relaxation times and high fluctuations in mWT cells due to lower cell-stiffness (relative to mE-cad KO) results in persistent and large compressive stresses, we relax the elastic contrast between mE-cad KO and mWT cells by reducing the mE-cad KO stiffness to that of mWT. In this case, the temporal evolution of field statistics reveal higher variance for mE-cad KO cells (Extended Fig. 7d), relative to the case with elastic contrast (Extended Fig. 7e). This results provide an insight on the interplay of cell stiffness, dominance of fluctuations, and localization of stresses which ultimately impacts the fate of an extruding cell.

3 Statistics

Statistical analysis of all the data sets are performed by student t-test and unpaired t-test which were implemented using Graphpad Prism and verified using Matlab. On the plots: n.s., not significant; *p<0.05; **p<0.01; ***p<0.001; and ****p<0.0001

References

1. Balasubramaniam, L. et al. Investigating the nature of active forces in tissues reveals how contractile cells can form extensile monolayers. en. Nature Materials **20,** 1156–1166. ISSN: 1476-4660. (2021) (2021).
2. Zhang, J. et al. Visualization of caspase-3-like activity in cells using a genetically encoded fluorescent biosensor activated by protein cleavage. Nature Communications **4,** 2157. ISSN: 2041-1723 (2013).
3. Eisenhoffer, G. T. et al. Crowding induces live cell extrusion to maintain homeostatic cell numbers in epithelia. eng. Nature **484,** 546–549. ISSN: 1476-4687 (2012).
4. Sabeh, F. et al. Tumor cell traffic through the extracellular matrix is controlled by the membrane-anchored collagenase MT1-MMP. Journal of Cell Biology **167,** 769–781. ISSN: 0021-9525. https://doi.org/10.1083/jcb.200408028 (2004).
5. Monteiro, P. et al. Endosomal WASH and exocyst complexes control exocytosis of MT1-MMP at invadopodia. Journal of Cell Biology **203,** 1063–1079. ISSN: 0021-9525 (2013).
6. Coussy, F. et al. A large collection of integrated genomically characterized patient-derived xenografts highlighting the heterogeneity of triple-negative breast cancer. International Journal of Cancer **145,** 1902–1912. ISSN: 1097-0215 (2019).
7. Padmanaban, V. et al. E-cadherin is required for metastasis in multiple models of breast cancer. Nature **573,** 439–444. ISSN: 1476-4687 (2019).

8. Yu, G., Wang, L.-G., Han, Y. & He, Q.-Y. clusterProfiler: an R Package for Comparing Biological Themes Among Gene Clusters. OMICS: A Journal of Integrative Biology **16,** 284–287 (2012).

9. Subramanian, A. et al. Gene set enrichment analysis: A knowledge-based approach for interpreting genome-wide expression profiles. Proceedings of the National Academy of Sciences **102,** 15545–15550 (2005).

10. Liberzon, A. et al. The Molecular Signatures Database Hallmark Gene Set Collection. Cell Systems **1,** 417–425. ISSN: 2405-4712 (2015).

11. Martiel, J.-L. et al. Measurement of cell traction forces with ImageJ. eng. Methods in Cell Biology **125,** 269–287. ISSN: 0091-679X (2015).

12. Berg, S. et al. ilastik: interactive machine learning for (bio)image analysis. Nature Methods **16,** 1226–1232. ISSN: 1548-7105 (2019).

13. Tinevez, J.-Y. et al. TrackMate: An open and extensible platform for single-particle tracking. Methods. Image Processing for Biologists **115,** 80–90. ISSN: 1046-2023 (2017).

14. Thielicke, W. PIVlab –Towards user friendly, affordable and accurate digital particle image velocimetry in MATLAB. Journal of Open Research Software **2,** 30 (2014).

15. Tseng, Q. et al. Spatial Organization of the Extracellular Matrix Regulates Cell-Cell Junction Positioning. en. Proceedings of the National Academy of Sciences **109,** 1506–1511 (2012).

16. Nier, V. et al. Inference of Internal Stress in a Cell Monolayer. Biophysical Journal **110,** 1625–1635. ISSN: 0006-3495 (Apr. 2016).

17. Monfared, S., Ravichandran, G., Andrade, J. & Doostmohammadi, A. Mechanical basis and topological routes to cell elimination. Elife **12,** e82435 (2023).

18. Hohenberg, P. C. & Halperin, B. I. Theory of dynamic critical phenomena. Reviews of Modern Physics **49,** 435–479. ISSN: 0034-6861. http://dx.doi.org/10.1103/RevModPhys.49.435 (July 1977).

19. Palmieri, B., Bresler, Y., Wirtz, D. & Grant, M. Multiple scale model for cell migration in monolayers: Elastic mismatch between cells enhances motility. Sci. Rep. **5,** 11745. ISSN: 2045-2322 (2015).

20. Physical models of cell motility 1st ed. en (ed Aranson, I. S.) (Springer International Publishing, Basel, Switzerland, Dec. 2015).

21. Camley, B. A. & Rappel, W.-J. Physical models of collective cell motility: from cell to tissue. Journal of Physics D: Applied Physics **50,** 113002 (2017).

22. Mueller, R., Yeomans, J. M. & Doostmohammadi, A. Emergence of Active Nematic Behavior in Monolayers of Isotropic Cells. Physical Review Letters **122** (Feb. 2019).

23. Prost, J., Jülicher, F. & Joanny, J.-F. Active gel physics. Nature physics **11,** 111–117 (2015).

24. Abercrombie, M. & Heaysman, J. E. Observations on the social behaviour of cells in tissue culture. Experimental Cell Research **6,** 293–306 (1954).

25. Abercrombie, M. Contact inhibition and malignancy. Nature **281,** 259–262 (1979).

26. Smeets, B. et al. Emergent structures and dynamics of cell colonies by contact inhibition of locomotion. Proceedings of the National Academy of Sciences **113,** 14621–14626 (2016).

27. Peyret, G. et al. Sustained Oscillations of Epithelial Cell Sheets. Biophysical Journal **117,** 464–478. https://doi.org/10.1016/j.bpj.2019.06.013 (2019).

28. Irving, J. H. & Kirkwood, J. G. The Statistical Mechanical Theory of Transport Processes. IV. The Equations of Hydrodynamics. The Journal of Chemical Physics **18,** 817–829. https://doi.org/10.1063/1.1747782 (June 1950).

29. Christoffersen, J., Mehrabadi, M. M. & Nemat-Nasser, S. A Micromechanical Description of Granular Material Behavior. Journal of Applied Mechanics **48,** 339–344. ISSN: 1528-9036. http://dx.doi.org/10.1115/1.3157619 (June 1981).

30. Chugh, P. et al. Actin cortex architecture regulates cell surface tension. Nature cell biology **19,** 689–697 (2017).

31. Taneja, N. et al. Precise tuning of cortical contractility regulates cell shape during cytokinesis. Cell reports **31** (2020).

32. Arciero, J. C., Mi, Q., Branca, M. F., Hackam, D. J. & Swigon, D. Continuum model of collective cell migration in wound healing and colony expansion. Biophysical journal **100,** 535–543 (2011).

33. Cochet-Escartin, O., Ranft, J., Silberzan, P. & Marcq, P. Border forces and friction control epithelial closure dynamics. Biophysical journal **106,** 65–73 (2014).

34. Priest, A. V. & Sivasankar, S. in Mechanobiology: Methods and Protocols 63–77 (Springer, 2023).

35. Trichet, L. et al. Evidence of a large-scale mechanosensing mechanism for cellular adaptation to substrate stiffness. Proceedings of the National Academy of Sciences **109,** 6933–6938 (2012).

36. Tan, S. J. et al. Regulation and dynamics of force transmission at individual cell-matrix adhesion bonds. Science Advances **6,** eaax0317 (2020).

37. Peyret, G. et al. Sustained oscillations of epithelial cell sheets. Biophysical journal **117,** 464–478 (2019).

38. Du Roure, O. et al. Force mapping in epithelial cell migration. Proceedings of the National Academy of Sciences **102,** 2390–2395 (2005).

39. Sonin, A. A. A generalization of the Π-theorem and dimensional analysis. Proceedings of the National Academy of Sciences **101,** 8525–8526 (2004).

40. Marquez-Florez, K., Arroyave-Tobón, S. & Linares, J.-M. From biological morphogenesis to engineering joint design: a bio-inspired algorithm. Materials & Design **225,** 111466 (2023).

41. Löber, J., Ziebert, F. & Aranson, I. S. Collisions of deformable cells lead to collective migration. Scientific Reports **5.** https://doi.org/10.1038/srep09172 (Mar. 2015).

42. Pérez-Calixto, D. et al. Determination by Relaxation Tests of the Mechanical Properties of Soft Polyacrylamide Gels Made for Mechanobiology Studies. Polymers **13,** 629. ISSN: 2073-4360. http://dx.doi.org/10.3390/polym13040629 (Feb. 2021).

a

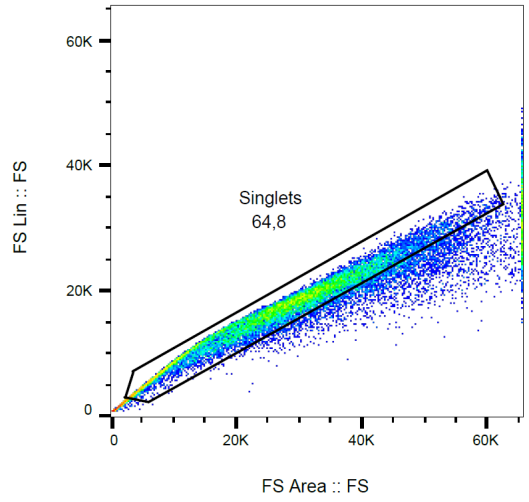
Singlets
64,8
FS Lin :: FS
FS Area :: FS
0
20K
40K
60K

b

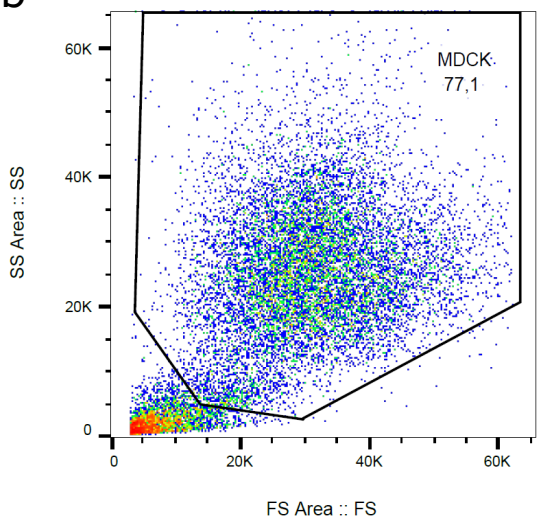
MDCK
77,1
SS Area :: SS
FS Area :: FS
0
20K
40K
60K

c

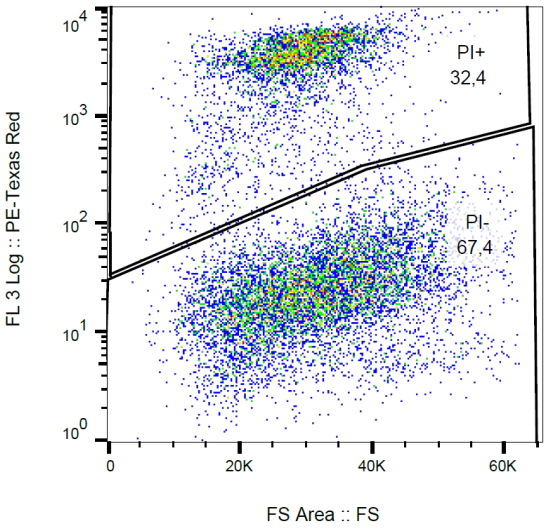
PI+
32,4
PI-
67,4
FL 3 Log :: PE-Texas Red
FS Area :: FS
10^0
10^1
10^2
10^3
10^4
0
20K
40K
60K

d

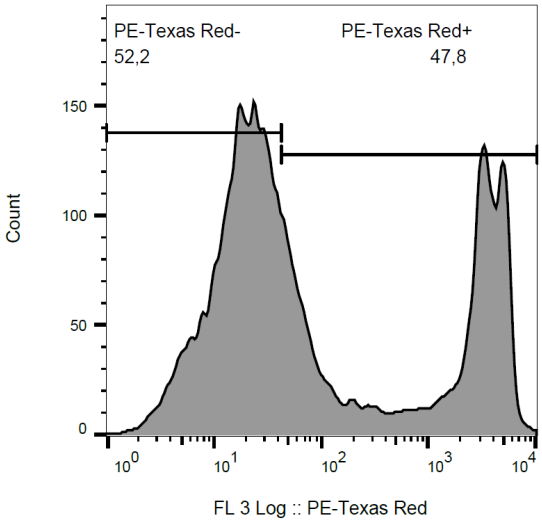
PE-Texas Red-
52,2
PE-Texas Red+
47,8
Count
FL 3 Log :: PE-Texas Red
0
50
100
150
10^0
10^1
10^2
10^3
10^4

Supplementary Figure 1: Gating strategy employed during flow cytometry analysis. a) Gating strategy employed to identify singlets from clumps of cells. b) Gating strategy employed based on area to filter out debris. c) Fluorescent intensity based gating employed to separate out dead (PI+) and live cells (PI-). d) Counts obtained from the gating strategy in c) to extract the number of PI+ and PI- cells.